Canadian Metallurgical Quarterly, Vol 42, No 4 pp 495-507, 2003

PHASE EQUILIBRIA, THERMODYNAMIC MODELLING AND NEUTRON DIFFRACTION OF THE AlN-Al_2O_3-Y_2O_3 SYSTEM

M. MEDRAJ[1], R. HAMMOND[2], W.T. THOMPSON[3] and R.A.L. DREW[4]

[1]Concordia University, Montreal, Quebec, Canada.
[2]NPMR, NRC, Chalk River, Ontario, Canada.
[3]Royal Military College of Canada, Kingston, Ontario, Canada.
[4]McGill University, montreal, Quebec, Canada

(Received April, 2003; in revised form July, 2003)

Abstract — Aluminum nitride (AlN) is usually sintered using yttria (Y_2O_3) as an additive where it reacts with the surface species to form a Y-Al-O-N liquid that promotes particle rearrangement and densification. Construction of the phase relations in this multicomponent system is important for the development of this ceramic. The ternary phase diagram of the AlN-Al_2O_3-Y_2O_3 was developed by Gibbs energy minimization using interpolation procedures based on the modelling of the binary subsystems. Binary diagrams of Al_2O_3-Y_2O_3, AlN-Al_2O_3, and AlN-Y_2O_3 were thermodynamically modelled. The calculated Gibbs energies of components, stoichiometric phases and solution parameters were used for the calculation of isothermal sections of the AlN-Al_2O_3-Y_2O_3 ternary system. Five ternary eutectic points occur in this system in the temperature range of 1776 to 1861 °C. The ternary phase diagram was thermodynamically modelled and experimentally verified for the first time in this work.

Résumé — Le nitrure d'aluminium (AlN) est habituellement fritté en utilisant de l'oxyde d'yttrium (Y_2O_3) comme additif où il réagit avec les espèces de la surface pour former un liquide de Y-Al-O-N qui stimule la réorganisation de particule et la densification. La construction des relations de phase de ce système à plusieurs constituants est importante pour le développement de cette céramique. Le diagramme de phase ternaire de l'AlN-Al_2O_3-Y_2O_3 a été développé par minimisation de l'énergie de Gibbs en utilisant des procédures d'interpolation basées sur la modélisation de sous-systèmes binaires. On a modélisé au moyen de la thermodynamique les diagrammes binaires Al_2O_3-Y_2O_3, AlN-Al_2O_3 et AlN-Y_2O_3. On a utilisé les énergies de Gibbs calculées pour les constituants, les phases stoechiométriques et les paramètres de solution pour le calcul de sections isothermes du système ternaire AlN-Al_2O_3-Y_2O_3. Il y a cinq points eutectiques ternaires dans ce système dans la gamme de température de 1776 °C à 1861 °C. On a modélisé le diagramme de phase ternaire au moyen de la thermodynamique et on l'a vérifié expérimentalement pour la première fois au cours de ce travail.

INTRODUCTION

Aluminum nitride (AlN) has been intensively studied due to its suitability as an electronic substrate since it offers high thermal conductivity, high flexural strength and is non-toxic [1].

Sintering of AlN with the addition of Y_2O_3 occurs in the presence of a liquid phase where the interaction between Y_2O_3 and the surface species of AlN powder forms a liquid during sintering [2]. The amount of liquid and the phase evolution at a selected sintering temperature can be predicted using phase equilibrium diagrams and thus highlights the importance of a detailed and complete study of the AlN-Al_2O_3-Y_2O_3 phase equilibrium.

To date, there is little information on the ternary AlN-Al_2O_3 sintering additives system [3] and, in spite of the large interest attracted over the last 10-15 years by the excellent properties of AlN sintered by Y_2O_3, no attempts have been made to construct the AlN-Al_2O_3-Y_2O_3 ternary phase diagram. To calculate reliable ternary, quaternary and higher order metallic and ceramic phase diagrams, a thermodynamic description of the binary phase diagrams is needed and a thermodynamic model that can extrapolate binary data reliably into ternary and higher order systems is required [4]. This is commonly done for metals where the thermodynamic data are more readily available. For ceramic systems, thermodynamic data are very sparse and furthermore, these measurements are very difficult to perform considering the high temperatures involved.

Experimental determination of phase diagrams is a time consuming and costly task especially when it involves high temperature. This becomes even more pronounced as the number of components increases. The calculation of phase diagrams reduces the effort required to determine equilibrium conditions in a multicomponent system and focuses experimental efforts on critical regions. A preliminary phase diagram can be obtained from the extrapolation of the thermodynamic functions of constituent subsystems and can be used to identify the composition and temperature regimes with limited experimental effort [5-7].

Al_2O_3-Y_2O_3 *Phase Diagram*

The significance of this phase diagram comes from the importance of alumina and yttria for liquid phase sintering of covalently bonded ceramics such as AlN, Si_3N_4 and SiC.

There are three aluminate compounds in this system: $Y_3Al_5O_{12}$ (YAG), $YAlO_3$ (YAP) and $Y_4Al_2O_9$ (YAM). These compounds are of considerable interest as solid state laser materials [8-10]. Cockayne [10] reviewed this system and reported the melting points and the stability ranges for the end and stoichiometric compounds that occur in this system. Warshaw and Roy were the first to study phase equilibria in this system in 1959. They considered YAP as a thermodynamically metastable compound and did not include it in their phase diagram. However, they did indicate the liquidus in this phase diagram with a dashed line [11,12]. Their phase diagram was measured using X-ray analysis and melting observations. The first estimate of thermodynamic functions of this system was published by Kaufman *et al.* [13] by employing the CALPHAD (CALculation of Phase Diagram) method. Gröbner *et al.* [8] optimized the system using all available experimental data in the literature.

AlN-Y_2O_3 *Phase Diagram*

No effort has been made to date to analyze the entire system experimentally. Kaufman *et al.* [13] published a thermodynamic estimation for this phase diagram. They reported that a simple eutectic phase diagram describes the equilibria in this system. Huang *et al.* [14] studied AlN-Nd_2O_3 and AlN-Eu_2O_3 binary systems. They reported that the AlN-Y_2O_3 system should have a similar phase diagram which contains a liquid region with a steep liquidus line from Y_2O_3 and a gaseous region on the AlN side.

AlN-Al_2O_3 *Phase Diagram*

The phase diagram of AlN-Al_2O_3 system was studied by several authors [15-25]. Qiu and Metselaar [15] reviewed the contradictory information obtained previously, reinvestigated the system and published an optimized phase diagram.

In general, knowledge of AlN-Al_2O_3 phase equilibria is based on that of the Si-Al-O-N quaternary system which has been studied intensively because of its importance in the sintering of Si_3N_4 and the formation of SiAlON compounds [16]. The first phase diagram for this system was reported by Lejus in 1964. Six phases were identified including a phase designated 'X' which encompassed all compositions for the polytype phases [17]. The phases which form in the AlN-Al_2O_3 system can be separated into two groups depending on their basic crystallographic structure. One group is based on polytypes of the wurtzite structure and the other is based on the spinel structure [17]. Qiu and Metselaar [15] calculated the binary AlN-Al_2O_3 system. The interaction parameters for the liquid were evaluated by applying the ionic liquid model. The thermodynamic descriptions of the ternary compounds (Al-O-N) are from the work of Dumitrescu and Sundman [22] where they used the substitutional model for the liquid. The phase relations were also calculated by Dorner *et al.* in 1981 and Kaufman in 1979 using thermodynamic data. Both investigations used a 25 mol% AlN for the composition of γ-spinel phase. The resulting calculated phase diagrams had γ-spinel as the only stable intermediate phase in the system [17]. On the other hand, Hillert and Jonsson in 1992 included 27R stoichiometric phase in their calculations in addition to considering the non-stoichiometry of the γ-spinel phase. They reported that 27R and γ-spinel melt congruently at 2998 K (2725 °C) and 2436 K (2163 °C), respectively [24]. Tabary and Servant [25] recently (1998) published a calculated AlN-Al_2O_3 phase diagram. In their calculation, the Gibbs energy of formation of the solution as well as compound phases in this system were derived from an optimization procedure using all the available experimental thermodynamic and phase diagram data. They used the sub-lattice model for the compounds which exhibited a range of non-stoichiometry and the Redlich-Kister polynomial for the solution phases.

THERMODYNAMIC MODELLING METHODOLOGY

Generally speaking, some differences in thermodynamic properties always exist between actual and ideal solution behaviour depending on the premises for the *ideal* mixing. Since there was no strong basis for the selection of the ideal Gibbs energy of mixing term based upon experimental knowledge of the structure of the solution phases, the choice was made to base it on the mole fraction of component oxide or nitride in all three sub-system solution phases. The excess Gibbs energy function was then adjusted accordingly to provide the Gibbs energy of the solution phase to fit the known phase diagram. Success and justification of this modelling approach was judged on the basis of two criteria. The first one is being able to represent the binary phase diagrams to the extent the current experimental understanding allows. The second is having a few

adjustable parameters in the expression of the excess Gibbs energy. Li *et al.* [26] earlier analyzed the phase diagrams of the Al_2O_3-SiO_2-R_2O_3 (where R= Nd, Sm) system using the same methodology. Also Fang *et al.* [27] used this approach to study thirteen binary systems of the form A_2CO_3-AX or A_2SO_4-AX (where A = Li, Na, K; X = Cl, F, NO_3, OH) and to calculate their binary phase diagrams.

The optimum accuracy of phase diagram modelling is obtained if all experimental data are taken into account and if thermodynamic consistency exists between all thermodynamic functions of the different phases and the phase diagram. If these functions are presented analytically, they can be extrapolated for systems with one additional component. If the analytical representation always uses the same standardized patterns, all the information of a system will be contained in a set of coefficients and will be easily stored [7].

A system is at equilibrium when its Gibbs energy is at a minimum. If we could calculate the Gibbs energy of all the possible phases of a system at a specified temperature as a function of composition, it would be a simple matter to select that phase or combination of phases which provides the lowest value of Gibbs energy for that system. By definition, these would be the equilibrium phases for the system at that temperature. By repetition of these calculations for the number of temperatures, the phase boundaries of the system can be determined and the phase diagram can be constructed [28]. Once the binary subsystems have been analyzed by a coupled thermodynamic/phase diagram analysis, the phase diagram of a ternary or a quaternary system can usually be calculated with a maximum error no greater than about twice that of the maximum error of the binary phase diagrams assuming that there is no strong ternary or quaternary interactions. Hence, in order to minimize the experimental effort, one should concentrate on remeasuring regions of the binary diagrams where required. The ternaries and quaternaries can then be recalculated [29].

$$G = \sum_{i=1}^{p} n_i G_i \qquad (1)$$

For the calculation of phase equilibria in a multicomponent system, it is necessary to minimize the total Gibbs energy, G, of all the phases that take part in this equilibrium where n_i is the number of moles of phase i, G_i is the Gibbs energy of phase i and p is the number of phases. All calculations in this study were performed with the aid of the F*A*C*T thermodynamic computer system [30].

Mathematical Expressions

Gibbs energies of fusion and melting points of Al_2O_3 and Y_2O_3 are taken from [8,30-32]. Mathematical expressions of Gibbs energy for the different phases were generated using regression methods. The experimental liquidus curves of the Al_2O_3-Y_2O_3 system [33] are the source of thermodynamic data for the liquid and for the stoichiometric compounds.

The Gibbs energy of a binary stoichiometric phase is given by

$$G^{\varphi} = x^0_{Al_2O_3} G^0_{Al_2O_3} + x^0_{Y_2O_3} G^0_{Y_2O_3} + \Delta G^f \qquad (2)$$

where $x^o_{Al_2O_3}$ and $x^o_{Y_2O_3}$ are mole fractions of Al_2O_3 and Y_2O_3 and are given by the stoichiometry of the compound, $G^o_{Al_2O_3}$ and $G^o_{Y_2O_3}$ are the respective reference states and ΔG^f is the Gibbs energy of formation.

The liquid phase is described as random mixtures of the components by a regular solution type model.

$$\begin{aligned} G^{\varphi} = {} & x_{Al_2O_3} G^0_{Al_2O_3} + x_{Y_2O_3} G^0_{Y_2O_3} \\ & + RT\left\{x_{Al_2O_3} \ln x_{Al_2O_3} + x_{Y_2O_3} \ln x_{Y_2O_3}\right\} \\ & + x_{Al_2O_3} x_{Y_2O_3} \sum_{j=1}^{M} k_j \left(x_{Al_2O_3} - x_{Y_2O_3}\right)^j \end{aligned} \qquad (3)$$

where $x_{A_2O_3}$ and $x_{Y_2O_3}$ are the mole fractions and $G^o_{A_2O_3}$ and $G^o_{Y_2O_3}$ are the reference states of Al_2O_3 and Y_2O_3, respectively. The k_j are coefficients of the excess Gibbs energy term. The sum of the terms $(x_A - x_B)^j$ is the so-called Redlich-Kister polynomial which is the most commonly used polynomial in regular solution type descriptions and M is the number of coefficients.

The coefficients k_j may be written as linear functions of temperature, T.

$$k_j = h_j - TS_j \qquad (4)$$

Hence, the integral molar enthalpy of mixing and the excess entropy of mixing, assumed independent of temperature, are given in terms of the coefficients *hj* and *Sj* as:

$$\Delta h = \sum_{j=1}^{M} h_j x^j_{Al_2O_3} \left(1 - x_{Al_2O_3}\right)^j \qquad (5)$$

$$S^E = \sum_{j=1}^{M} S_j x^j_{Al_2O_3} \left(1 - x_{Al_2O_3}\right)^j \qquad (6)$$

where *M* is the total number of such coefficients [29]. Although other polynomials have been used in the past, in most cases they can be converted to Redlich-Kister polynomials [5].

So far we have mathematical expressions for the phases in Al_2O_3–Y_2O_3. The same procedure was followed for the Al_2O_3–AlN system. The phase diagram of Qiu and Metselaar [15] and Gibbs energy of fusion of the two pure components were used to model this phase diagram. Gibbs energy of fusion and the hypothetical melting point of AlN were taken from Reference 13.

As mentioned earlier, there is no experimental phase diagram available for the AlN–Y_2O_3 system in the literature. So this system was predicted using the Gibbs energies of fusion of the two pure components, AlN and Y_2O_3, which were already used to calculate the other two binary systems in addition to the eutectic point at 14.5 wt% AlN reported by Kaufman *et al.* [13].

Validity of the Models

From the mathematical expressions of the Gibbs energy of each phase as a function of temperature and composition and by calculating (the lowest common tangents) to the Gibbs energy composition curves, graphical presentation of the binary phase diagram can be generated. By comparing these diagrams with the experimental phase diagrams, the mathematical models can be examined and adjusted until agreement is achieved.

Database for AlN-Al_2O_3-Y_2O_3 *System*

There is an increasing demand for the development of thermodynamic databases which are of practical use. A simple model which achieves this end is preferable to one which is unnecessarily complex and is based on speculation about the ionic structure of the phases. The goal is to identify the line between necessary and unnecessary complexity [34]. The aim of this work is to develop a thermdynamic data base which can be used to aid the processing of AlN.

The storage, retrieval and manipulation of thermodynamic data with the aid of computers require accurate analytical representation of thermodynamic properties of solutions. Values of the standard Gibbs energies, G^o, of each component are entered and stored in the solution database along with parameters which define the Gibbs energy of mixing according to Kohler-Toop polynomial model. Binary terms of the polynomial expansion were entered as Redlich-Kister polynomials due to their simplicity and the fact that their functional form is consistent with the empirical observations of solutions behaviour [35].

EXPERIMENTAL

To investigate the phase evolution in AlN-Al_2O_3-Y_2O_3 and in the binary systems experimentally, neutron diffraction patterns were monitored in situ at elevated temperatures using the DUALSPEC high resolution powder diffractometer, C2, at the NRU reactor of Atomic Energy of Canada Limited (AECL) Chalk River Laboratories. The diffractometer is an 800 channel position sensitive detector that spans 80° in scattering angle, 2θ. The wavelength, λ, of the neutron beam was calibrated by measuring the diffraction pattern of a standard powder of alumina obtained from the National Institute of Standards and Technology. λ = 1.33(1) Å and 2θ range from 8° to 88° were used in this experiment. The diffractometer was equipped with a tantalum element vacuum furnace capable of reaching temperatures as high as 2000 °C.

AlN (Tokuyama Soda, grade F), Y_2O_3 (Molycorp, grade 5600) and Al_2O_3 powder (Alcoa, grade A16-SG) were mixed in various stoichiometric amounts. Table I and Figures 6 to 9 show the composition of these samples. It can be seen from these figures that the compositions were selected carefully to be close to the phase boundaries in order to critically verify the thermodynamic findings. In situ neutron diffraction was performed during the heating and cooling of these samples by monitoring the changes in the diffraction peaks and the diffraction angles. In this paper, only composition 1 and 6 (the eutectic composition in AlN-Y_2O_3), will be discussed. Detailed experimental investigation of the ternary system is in Reference 36.

Table I – The chemical composition of the studied samples

Sample no.	Composition (mol%)		
	AlN	Al_2O_3	Y_2O_3
1	12	74	14
2	17.5	64	18.5
3	24	70	6
4	7	33	60
5	33	20	47
6	47	0	53

A neutron diffraction spectrum for each sample was collected at room temperature to form the reference for any reactions taking place upon heating. The evolution of the reactions was followed by incrementally raising the temperature and maintaining it at temperature for 120 minutes to ensure that the reaction was complete. Cooling was also carried out in steps to detect the crystallization as well as the stability of each phase. Heating and cooling profiles were determined for each sample according to critical points which were predicted by the thermodynamic calculations. The samples were heated in nitrogen gas to prevent the decomposition of AlN.

RESULTS AND DISCUSSION

Al_2O_3-Y_2O_3 *Phase Diagram*

The calculated phase diagram of the Al_2O_3-Y_2O_3 system is shown in Figure 1. This diagram was calculated from the database built for the AlN-Al_2O_3-Y_2O_3 system. In this binary phase diagram there are three intermediate solid compounds, $Y_4Al_2O_9$, $YAlO_3$ and $Y_3Al_5O_{12}$, which will be referred to as YAM, YAP and YAG, respectively.

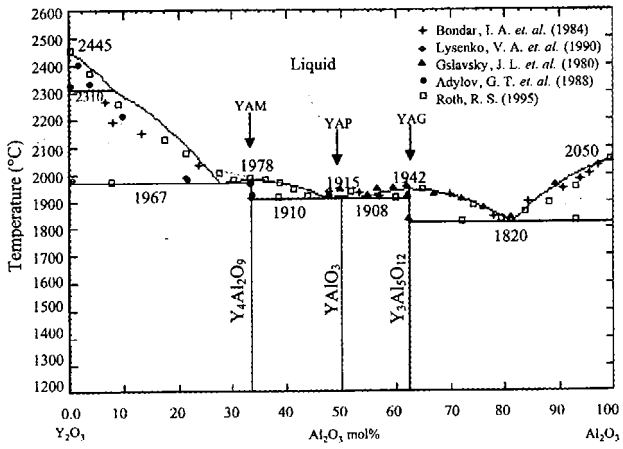

Fig. 1. Calculated Y_2O_3-Al_2O_3 phase diagram with experimental data from the literature.

Agreement between the calculated Al_2O_3-Y_2O_3 phase diagram and measured liquidus and other critical points is shown in Figure 1. The calculated eutectic composition and temperature agree with the experimental values from the literature. This indicates that the thermodynamic model is capable of reproducing the measured phase diagram within experimental error limits. In a very recent study, Fabrichnaya *et al.* [37] used high temperature drop solution calorimetry measurements and phase equilibria to assess the thermodynamic functions in the Al_2O_3-Y_2O_3 system. Their calculated phase diagram agrees with the measurements. Comparison between their results and the results of this work is given in Table II. Overall, the current calculated phase diagram is in good agreement with these results.

AlN - Al_2O_3 *Phase Diagram*

The optimized phase diagram of AlN-Al_2O_3 system in relation to experimental data from the literature is shown in Figure 2. Since experimental data are never self-consistent, a decision as to which data one wishes to emphasize is inescapable. The most recent experimental results for AlN-Al_2O_3 were chosen for these purposes. The present analysis is in excellent agreement with the experimental results from the literature.

The resultant melting point of pure AlN agrees with the hypothetical melting temperature of AlN, 2794 °C, report-

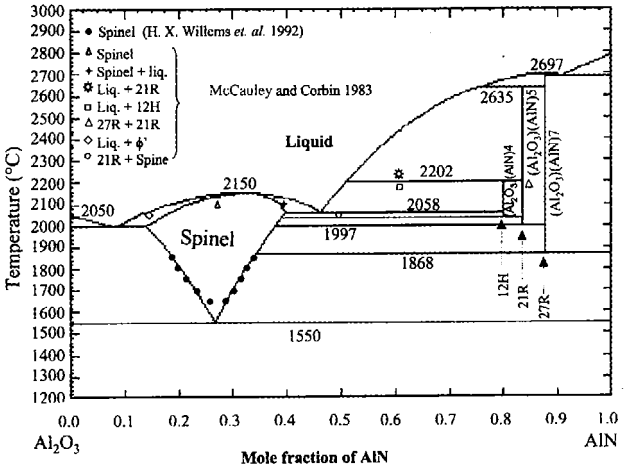

Fig. 2. Calculated Al_2O_3-AlN phase diagram with experimental data from the literature.

Table II – Comparison of phase equilibrium results of the Al_2O_3-Y_2O_3 system

Reaction	Current work (Al_2O_3 mol%, T °C)	Fabrichnaya *et al.* [37] (Al_2O_3 mol%, T °C)
YAG + Al_2O_3 → liq	(80, 1820)	(80.28, 1810)
YAG + YAP → liq	(54, 1908)	(54.5, 1900)
YAP + YAM → liq	(47, 1910)	(46.7, 1903)
YAM + Y_2O_3 → liq	(28, 1967)	(25.6, 1948)
YAG → liq	(37.5, 1942)	(37.5, 1923)
YAG → liq	(50, 1915)	(50, 1907)
YAG → liq	(67, 1978)	(67, 1977)
Al_2O_3 → liq	(100, 2050)	(100, 2054)
Y_2O_3 → liq	(0, 2445)	(0, 2438)
Y_2O_3 BCC→ Y_2O_3 FCC	(92, 2310)	(92, 2327)

ed in Reference 24. γ-spinel was reported to melt congruently at 2165 °C in one atmosphere of nitrogen [17,25]. The present model shows that γ-spinel melts congruently at 2150 °C. Moreover, Ish-Shalom observed that at 1580°C, γ-spinel and AlN can be formed by the carbothermal reduction of aluminum oxide in nitrogen [23]. However, Lejus suggested that below 1600 °C γ-spinel decomposes into AlN and Al_2O_3. It can be seen that these results agree with the phase diagram obtained from the present model.

AlN - Y_2O_3 *Phase Diagram*

The AlN-Y_2O_3 phase diagram is a simple eutectic type. The calculated equilibrium phase diagram is shown in Figure 3.

In the optimization of the AlN-Y_2O_3 system, a high weighting factor was applied to the eutectic point. This choice was made on the basis that the eutectic temperature and composition are the only data available in the literature for this binary system. Figure 3 shows that the eutectic point is at X_{AlN} = 47 mol% and 1942 °C, which is very close to what Kaufman *et al.* [13] reported, X_{AlN} = 48.3 mol% and 1942 °C, for the eutectic composition and temperature, respectively. Decomposition of AlN was incorporated in Figure 3. It can be seen that at $P_{N2}+P_{Al}$ = 1 atm. AlN decomposes at 2600 °C. Kaufman *et al.* reported that AlN decomposes into Al and N_2 at 1 atm. above 2577 °C. This generally agrees with the decomposition temperature that results from the current assessment. Huang *et al.* [14] reported that no binary compound exists in this system and the eutectic temperature and composition 1730 °C and 20 mol% AlN, respectively. The eutectic temperature and composition contradict the results of Kaufman *et al.* [13] and the experimental results of this work.

High temperature *in situ* neutron diffraction experiments were conducted in order to study the phase relations obtained in the calculated AlN-Y_2O_3 binary phase diagram.

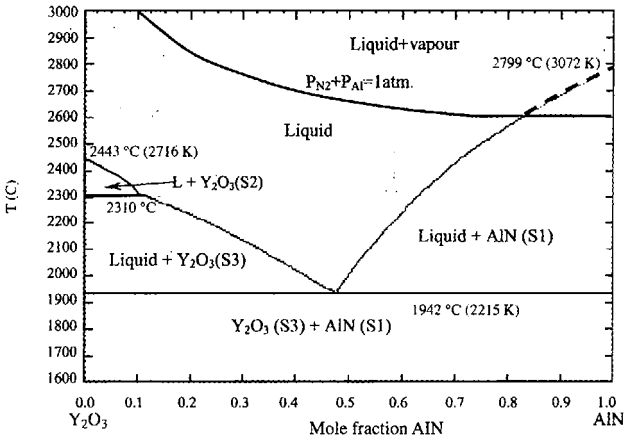

Fig. 3. Calculated AlN-Y_2O_3 phase diagram.

Diffraction patterns obtained during heating of the eutectic composition (47 mol% AlN) are shown in Figure 4.

Upon heating, the patterns are unchanged up to 1950 °C except for the shift due to lattice thermal expansion. AlN and Y_2O_3 are the only phases which exist from room temperature to melting which means that no reaction takes place between AlN and Y_2O_3 up to the melting point. Since this composition lost crystallinity at 2000 °C, then the melting point is between 1950 °C and 2000 °C.

$$AlN + Y_2O_3 \rightleftarrows \text{Liquid} \qquad (7)$$

Since melting occurred when the two solid phases were transformed directly into a liquid phase, then it appears that 47 mol% AlN is very close to the eutectic composition. The calculated eutectic temperature of AlN-Y_2O_3 is 1942 °C and the difference is within experimental uncertainty (±20 °C).

Neutron diffraction patterns were also collected during the cooling of this sample. AlN and Y_2O_3 were completely crystallized by cooling to 1900 °C. Hence, Y_2O_3 and AlN are the products of the eutectic reaction when Equation 5 is reversed upon cooling. AlN and Y_2O_3 are the only phases that exist down to room temperature. This proves that the phase relation between AlN and Y_2O_3 can be described by a simple binary eutectic phase diagram and there is no reaction between these two solids. This fact, as well as the measured eutectic temper-

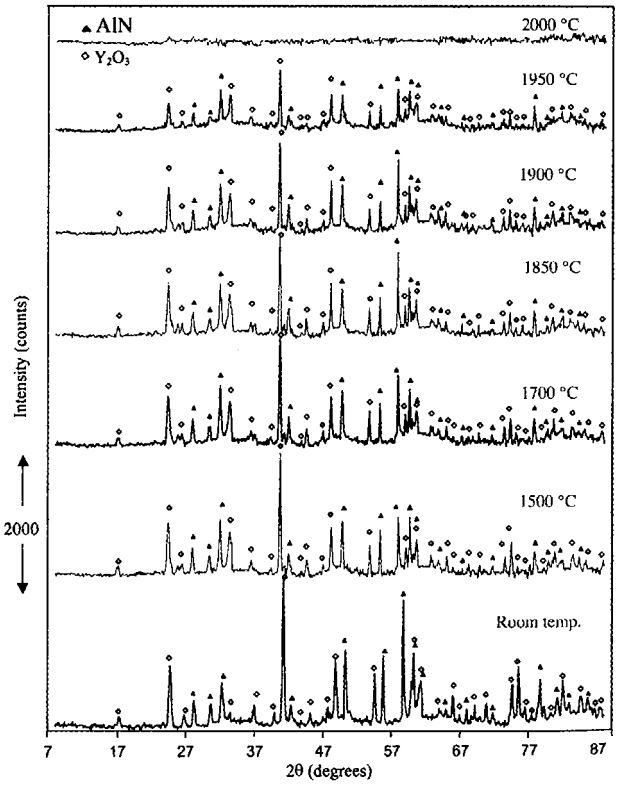

Fig.4. Neutron diffractograms during heating of AlN - Y_2O_3 eutectic composition.

ature are in good agreement with the calculated phase diagram for this system.

Isothermal Sections of AlN-Al_2O_3-Y_2O_3 *System*

Isothermal sections are calculated directly from the constructed database for the AlN-Al_2O_3-Y_2O_3 system. The ternary phase diagrams were calculated by assuming the ternary parameters to be zero and taking all the thermodynamic data available for the binary phases into consideration. The calculated isothermal sections of the AlN-Al_2O_3-Y_2O_3 system from 2500 °C down to 1700 °C are given in Figures 5 to 9.

At a very high temperature prior to solidification, the whole triangle would be composed of a homogeneous melt with no phase boundaries. However, 2500 °C is below the primary crystallization of AlN but still above the melting point of the other two components (Figure 5). This isothermal section shows that besides the region of homogenous melt, heterogeneous regions of the primary crystallization of AlN and AlN-based polytypes exist in equilibrium with the liquid phase. In addition, there are two small areas of L+27R+AlN and L+21R+27R. These regions of the melt and two crystalline types are the result of the binary eutectic crystallization of AlN and 27R according to

$$L \rightarrow AlN+27R \quad (8)$$

and of the binary peritectic crystallization of 27R and 21R which occurs according to

$$L+27R \rightarrow 21R+27R \quad (9)$$

By cooling from 2500 to 2000 °C (Figure 6), further primary solidification of different phases takes place and instead of three, there are five regions of primary solidification in which the crystalline types AlN, Y_2O_3, 27R, γ-spinel and Al_2O_3 occur in equilibrium with the liquid phase.

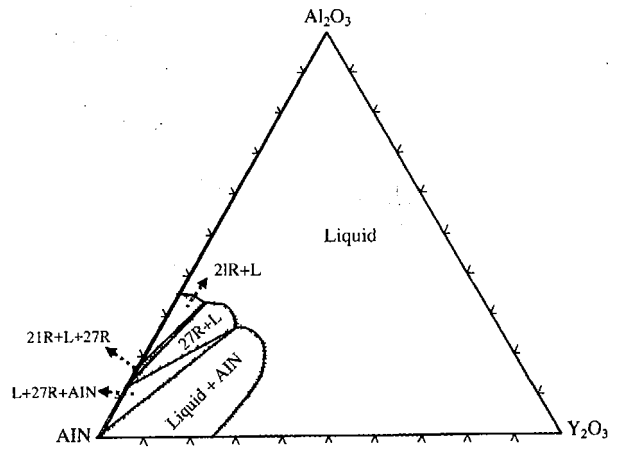

Fig. 5. Isothermal section at 2500 °C.

In Figure 6, tie lines are drawn in the two-phase region. It can be noticed that they rotate gradually from the orientation of the bounding tie lines. Compositions and proportional amounts of the conjugate phases for a particular composition can be obtained using the tie line that passes through the particular composition point, since the two phases have fixed composition but different proportions along the tie line.

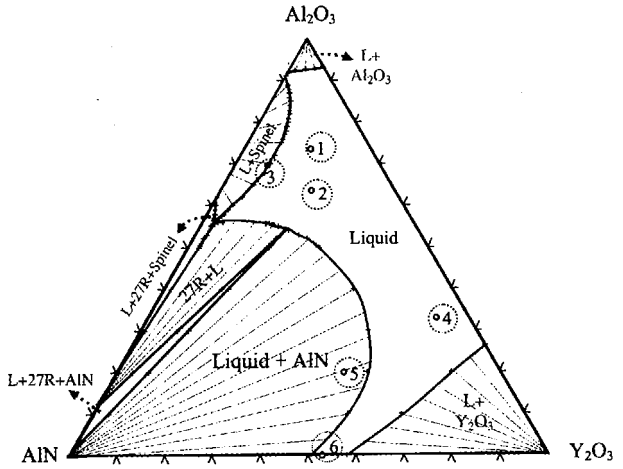

Fig. 6. Isothermal section at 2000 °C with the investigated compositions.

Two binary eutectic points have been encountered by cooling to 2000 °C. These are

$$L \rightarrow \gamma\text{-spinel}+27R \quad (10)$$

$$L \rightarrow 27R+AlN \quad (11)$$

At 1900 °C, most of the binary eutectic points of the system have appeared as shown in Figure 7. There are seven areas of binary eutectic crystallization corresponding to the following eutectic reactions:

$$L \rightarrow AlN+Y_2O_3 \quad (12)$$

$$L \rightarrow Y_2O_3+YAM \quad (13)$$

$$L \rightarrow YAP+YAG \quad (14)$$

$$L \rightarrow YAP+YAM \quad (15)$$

$$L \rightarrow AlN+27R \quad (16)$$

$$L \rightarrow \gamma\text{-spinel}+27R \quad (17)$$

$$L \rightarrow \gamma\text{-spinel}+Al_2O_3 \quad (18)$$

Furthermore, primary solidification for YAM, YAP and YAG occurs at this temperature.

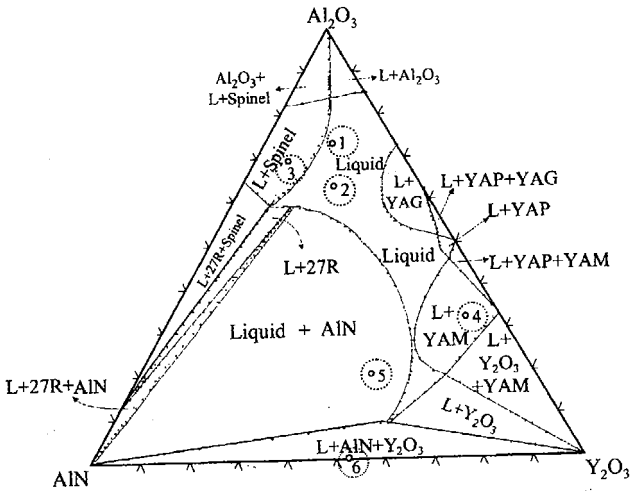

Fig. 7. Isothermal section at 1900 °C with the investigated compositions.

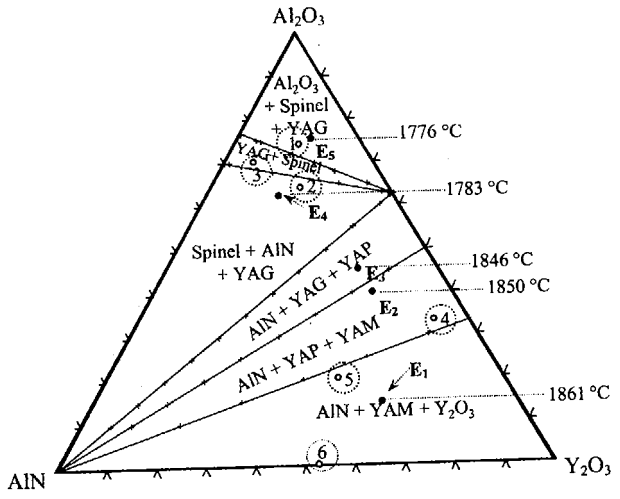

Fig. 9. Isothermal section at 1700 °C with the investigated compositions.

At 1800 °C, the isothermal section can be seen in Figure 8 indicating that the melt region has shrunk very significantly. However, some liquid is still in equilibrium with other phases and is contained in the two and three phase regions. The eutectic point between Al_2O_3 and YAG has been reached given the existence of the L+YAG+Al_2O_3 region is according to the following eutectic reaction.

$$L \rightarrow YAG+Al_2O_3 \quad (19)$$

Moreover, there are still regions of primary solidification of AlN, YAG, γ-spinel and Al_2O_3 in equilibrium with their respective melt. Figure 8 shows three regions of three solid phases. These indicate that three ternary eutectic points have been encountered upon cooling to this temperature and they are result of the following reactions:

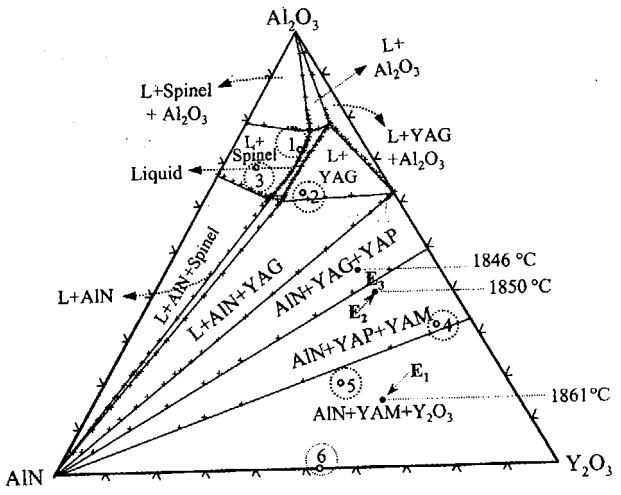

Fig.8. Isothermal section at 1800 °C with the investigated compositions.

$$L \rightarrow YAM+Y_2O_3+AlN \quad (20)$$

$$L \rightarrow YAM+YAP+AlN \quad (21)$$

$$L \rightarrow YAP+YAG+AlN \quad (22)$$

The first ternary eutectic point has a composition of 27.5 mol% AlN, 14.5 mol% Al_2O_3, 58.0 mol% Y_2O_3 and occurs at 1861 °C, whereas, the second and third ternary eutectic points have compositions of 16.0 mol% AlN, 40.0 mol% Al_2O_3, 44.0 mol% Y_2O_3 and 16.1 mol% AlN, 45.4 mol% Al_2O_3 and 35.5 mol% Y_2O_3 and occur at 1850 °C and 1846 °C, respectively.

At 1700 °C, there is no residual liquid and five three-crystalline phases regions and one two crystalline-phases region exist. This means that there are two other ternary eutectic points that have been encountered upon cooling to 1700 °C. They are calculated to occur at 1783 °C and 1776 °C according to the following reactions:

$$L \rightarrow \gamma\text{-spinel}+YAG+AlN \quad (23)$$

$$L \rightarrow \gamma\text{-spinel}+YAG+Al_2O_3 \quad (24)$$

In Situ Neutron Diffraction of AlN-Al_2O_3-Y_2O_3 *System*

Diffraction patterns obtained during the heating and cooling of composition 1 are shown in Figures 10 and 11. The patterns are shifted by a suitable offset for better comparison. The peaks are identified by markers given in the legend of each figure and will be discussed and compared with the thermodynamic findings in this section. The effect of thermal expansion was observed in all the samples when

the peaks shifted to lower and higher diffraction angles due to heating and cooling, respectively.

The reaction of this composition during heating from room temperature until 1900 °C is illustrated in Figure 10.

Increasing the temperature to 1200 °C did not introduce any change in the neutron diffraction pattern and indicated that no reaction took place in this temperature range. The first changes were visible when comparing the neutron diffraction patterns at 1200 °C and those at 1700 °C, where additional peaks appeared and were found to belong to YAG and γ-spinel. Unlike Al_2O_3 diffraction peaks, Y_2O_3 peaks were not observed at 1700 °C. This means that all the 14 mol% Y_2O_3 reacted to produce the YAG phase, whereas residual Al_2O_3 showed incomplete reaction to form γ-spinel. This is consistent with the ternary phase diagram shown in Figure 9 where composition 1 lies in the three-phase region of Al_2O_3, γ-spinel and YAG. Cheng *et al.* [39] also observed an incomplete reaction between Al_2O_3 and AlN at 1650 °C for 6 hours. They noticed an increase in the amount of γ-spinel with increasing time from 1 to 6 hours. Moreover, Yawei *et al.* [40] concluded that it is difficult to produce γ-spinel by reaction sintering below 1650 °C.

Upon heating from 1700 °C to 1800 °C, no difference in the diffraction patterns was observed. Neutron diffraction patterns were acquired at higher temperatures to detect liquid formation and melting. At 1850 °C, YAG was not observed, whereas γ-spinel was present. Since no other peaks were present at this temperature, it can be concluded that liquid formation started between 1800 and 1850 °C. This is consistent with the isothermal section calculated at 1800 °C (Figure 8).

It can be seen from Figure 10 that this composition lost crystallinity and became liquid at 1900 °C. Hence, melting occurred between 1850 and 1900 °C, and is consistent with the calculated isothermal section at 1900 °C shown in Figure 7.

Figure 11 shows the cooling cycle for composition 1. It can be seen that γ-spinel was fully crystallized by 1850 °C which confirms that the liquidus is in the temperature range of 1850 to 1900 °C. However, the diffraction pattern collected at 1800 °C did not reveal YAG as in the 1800 °C pattern collected during heating. In general, it was observed that the diffraction patterns during the cooling cycle are weaker than those collected during heating and is caused by sample shrinkage after melting. Also, the background of the patterns collected during cooling was higher than those obtained during the heating cycle. Moreover, YAG peaks produced lower absolute counts than γ-spinel and may have contributed to their disappearance into the pattern background at 1800 °C.

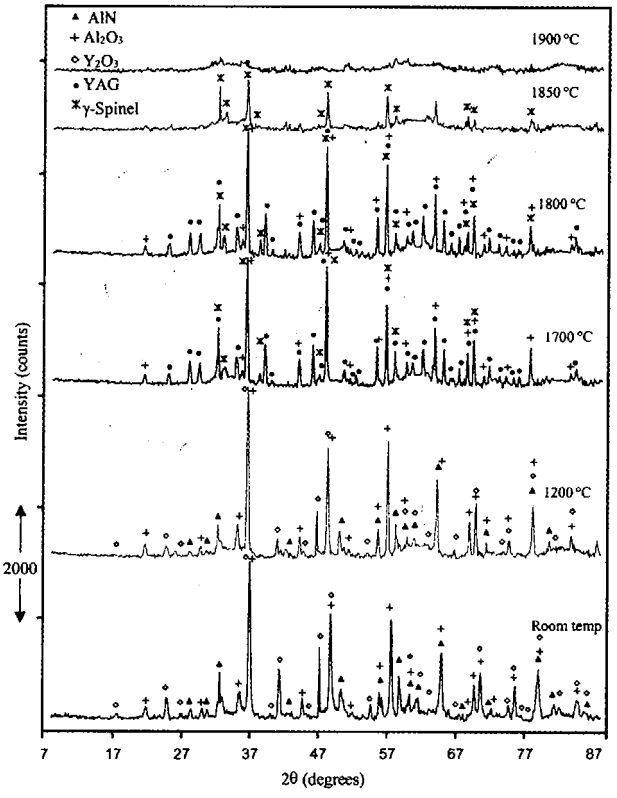

Fig.10. Neutron diffractograms during heating of composition 1.

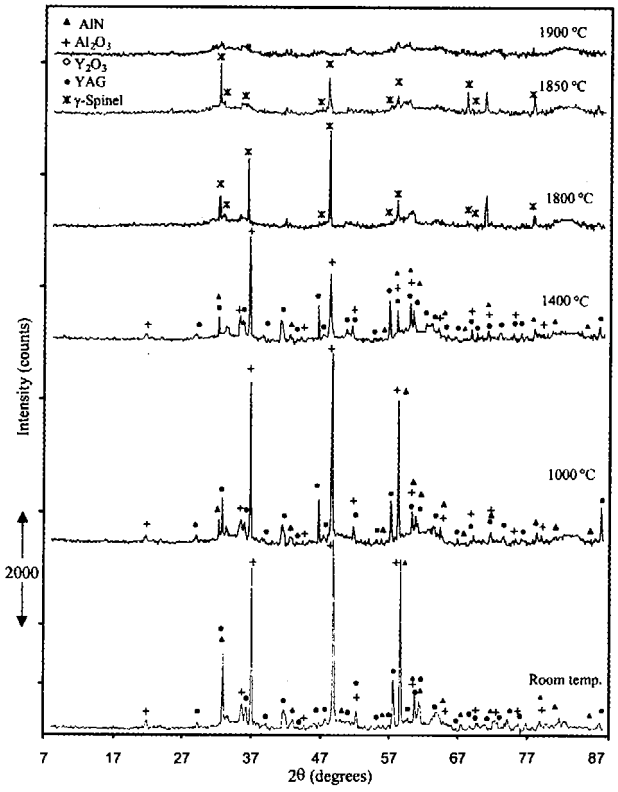

Fig. 11. Neutron diffractograms during cooling of composition 1.

By cooling to 1400 °C, decomposition of γ-spinel phase had occurred. This was evident by the new peaks of AlN and Al_2O_3 detected at this temperature. YAG peaks were observed in the diffraction pattern collected at 1400 °C. The same phases were found at 1000 °C but with stronger peaks for AlN and Al_2O_3 indicating further decomposition of γ-spinel upon cooling. The patterns obtained at 1000 °C and at room temperature were similar and were composed of AlN, YAG and Al_2O_3 upon reaching room temperature.

During the course of the present research, high temperature neutron diffraction was carried out for the binary systems and other ternary compositions [36], but are beyond the scope of the current paper. It was found that thermodynamic calculations generally agree with the experimental results.

CONCLUSIONS

From the results of this work, the following conclusions can be drawn:

1. The phase diagrams of the AlN-Al_2O_3-Y_2O_3 system were calculated based on the Kohler-Toop polynomial model. The three binary systems were first optimized and then phase diagrams of the ternary system were predicted from the optimized model parameters.

2. Calculated binary phase diagrams from the thermodynamic parameters reproduce the experimentally measured values very closely.

3. Experimental investigation of the equilibria in the AlN-Y_2O_3 system was performed using high temperature in situ neutron diffraction. The system is a simple eutectic phase diagram with a eutectic temperature between 1950 ± 20 °C and 2000 ± 20 °C and at a composition of 47 mol% AlN.

4. Five ternary eutectic points occur in this system in the temperature range of 1776 °C to 1861 °C.

5. An optimized self-consistent thermodynamic database has been developed. This database can now be used to predict the phase relations and various thermodynamic properties in this three-component system which represents AlN sintering.

6. High temperature neutron diffractometry has permitted real time reaction studies in the AlN-Al_2O_3-Y_2O_3 system, especially to determine the temperature range of each reaction, which would have been impossible by any other means.

ACKNOWLEDGEMENTS

This study was carried out with the support of a NSERC Strategic Project grant. The authors are indebted to the opportunity provided by NPMR-NRC in Chalk River to conduct the high temperature *in situ* neutron diffraction experiments.

REFERENCES

1. O.N. Grigoriev, S.M. Kushnerenko, K.A. Plotnikov and W. Kreher, *Advances in X-ray Analysis*, 1995, vol. 38, pp. 479-487.

2. M. Medraj, M. Entezarian and R.A.L. Drew, *Sintering 99 Conference Proceedings*, 2000, pp. 307-312.

3. N.H. Kim, K. Komeya and T. Meguro, *J. Mater. Sci*, 1996, vol. 31(6), pp. 1603-1608.

4. M. Hotch, *J. Phase Equilibria*, 1993, vol. 14(6), pp. 710-717.

5. U.R. Kattner, *JOM, 1007*, vol. 49(12), pp. 14-19.

6. M. Hillert, NATO ASI Series E Applied Science – Advanced Study Institute, 1994, [276], pp. 113-124.

7. H.L. Lukas, E.T. Henig and B. Zimmermann, CALPHAD, 1977 vol.3(1), pp. 225-236.

8. J. Gröbner, H.L. Lukas and F Aldinger, *Z. Metallkd.*, 1996, vol. 87(4), pp. 268-273.

9. J.S. Abell, I.R. Harris, B. Cockayne and B. Lent, *J. Mater. Sci.*, 1974, vol. 9, pp. 527-537.

10. B. Cockayne, *J. Less-Common Met.*, 1985, vol. 114, pp. 199-206.

11. Warshaw and R. Roy, *J. Am. Ceram. Soc.*, 1959, vol. 9(42), pp. 434-438.

12. A.A. Maier and I.G. Savinova, *Inorg. Mater.*, 1996, vol. 32(10), pp. 1078-1080.

13. L. Kaufman, F. Hayes and D. Birnie, CALPHAD, 1981, vol. 3(5), pp. 163-184.

14. Z.H. Huang and T.Y. Tien, *J. Am. Ceram.* Soc., 1996, vol. 79(6), pp. 1717-1719.

15. C. Qiu and R. Metselaar, *J. Am. Ceram.* Soc. 1997, vol. 80(8), pp. 2013-2020.

16. P. Tabary and C. Servant, *J. Appl. Cryst.*, 1999, vol. 32, pp. 241-252.

17. N.D. Corbin, *J. Europ. Ceram. Soc.*, 1989, vol. 5, pp.143-154.

18. J.W. McCauley and N.D. Corbin, *J. Am. Ceram. Soc.*, 1979, vol. 62(9-10), pp. 476-479.

19. J.W. McCauley and N.D. Corbin, *Progress in Nitrogen Ceramics*, 1983, pp. 111-118.

20. H. Fukuyama, W. Nakao, M. Susa and K. Nagata, *J. Am. Ceram. Soc.*, 1999, vol. 82(6), pp. 1381-1387.

21. H.X. Williems, G. De With and R. Metselaar, *J. Mater. Sci. Lett.*, 1993 , vol. 12, pp. 1470-1472.

22. L. Dumitrescu and B. Sundman, *J. Eur. Ceram. Soc.*, 1995, vol. 15(3), pp. 239-247.

23. H. X. Williems, M.M.R.M. Hendrix, R. Metselaar and G. De Wit, *J. Eur. Ceram. Soc.*, 1992, vol. (10), pp. 327-337.

24. M. Hillert and S. Jonsson, Z. *Metallkd,* 1992, vol. (83), pp. 714-719.

25. P. Tabary and C. Servant, CALPHAD, 1998, vol. 2(22), pp. 179-201.

26. L. Li, Z. Tang, W. Sun and P. Wang, *Phys. Chem. Glasses,* 1997, vol. 6(38), pp. 323-326.

27. Z. Fang and L. Chen, *Phys. Stat. Sol. A, Appl. Res.*, 1993, vol. 140(1), pp. 109-117.

28. Bergeron and Risbud, Introduction to Phase Equilibria in Ceramics, The American Ceramic Society, Inc. 1984, Reading.

29. C.W. Bale and A.D. Pelton, CALPHAD, 1982, vol. 4(6), pp. 253-278.

30. C.W. Bale, A.D. Pelton and W.T. Thompson, Facility for the Analysis of Chemical Thermodynamics, 1996, McGill University/Ecole Polytechnique.

31. M. Gervais, S. Le Floch, J.C. Rifflet, J. Coutures and J.P. Coutures, *J. Am. Ceram. Soc.*, 1992, vol. 75(11), pp. 3166-3168.

32. V.A. Lysenko, *Inorg. Mater.*, 1996, vol. 4(32), pp. 392-396.

33. R.S. Roth, Phase Equilibria Diagrams: Phase Diagrams for Ceramics, 1995, Volume XI, The American Ceramic Society, 107.

34. B. Burton, T.B. Chart, H.L. Lukas, A.D. Pelton, H. Seifert and P. Spencer, CALPHAD, 1995, vol. 4(19), pp. 537-553.

35. C.W. Bale and A.D. Pelton, *Metall. Trans.*, 1974, vol. 5, pp. 2323-2337.

36. M. Medraj, "Phase Equilibria in the AlN-Al_2O_3-Y_2O_3 System: Utility in AlN Processing", 2001, Ph.D. Thesis, McGill University.

37. O. Fabrichnaya, H.J. Seifert, R. Weiland, T. Ludwig, F. Aldinger and A. Navrotsky, *Z. Metallkd,* 2001, vol. 92(9), pp. 1084-1097.

38. T. Mah and M.D. Petry, *J. Am. Ceram. Soc.*, 1992, vol. 75(7), pp. 2006-2009.

39. J. Cheng, D. Agrawal and R. Roy, *J. Mater. Sci. Lett.*, 1999, vol. 18, pp. 1989-1990.

40. L. Yawei, L. Nan and Y. Runzhang, *J. Mat. Sci.*, 1997, vol. 32, pp. 979-982.

APPENDIX

Thermodynamic Data for AlN-Al_2O_3-Y_2O_3 *System*

The absolute enthalpy changes, entropies and Cps of Al_2O_3 and Y_2O_3 in their standard conditions at 298 K are tabulated in Table A-I.

Thermodynamic properties of the stoichiometric compounds in AlN-Al_2O_3-Y_2O_3 system are shown in Table A-II.

Values of the standard Gibbs energies, G^o, of each component are entered and stored in the solution database along with parameters which define the Gibbs energy of mixing according to the Kohler-Toop polynomial model and as shown in Table A-III.

The Redlich-Kister polynomial term in binary system M-N is defined as

$$G^E = X_M^l \, X_N^J \, (A + BT + CT \ln T)$$

In Table A-V, the G^E terms for the AlN-Al_2O_3-Y_2O_3 system are given as Redlich-Kister polynomials, where M and N are defined by the component number shown in Table A-IV.

Values of the standard Gibbs energy, G^o, for AlN and Al_2O_3 components summarized in Table A-V are entered and stored in the solution database with parameters that define the Gibbs energy of mixing according to the Kohler-Toop polynomial model as shown in Table A-VI.

Table A-I – Thermodynamic properties of AlN, Al_2O_3 and Y_2O_3

Reference phase	ΔH°_{298} (J)	S°_{298} (J/K)	Cp (J/K)
AlN (S1)	-317984	20.142	$50.4165 - 1665496.46T^{-2} + 7861.955T^{-1} + 232.265T^{-1/2} + 300647796\,T^{-3}$
Al_2O_3 (S4)	-1675700	50.82	$155.018 + 3861363T^{-2} + 828.3869T^{-1/2} + 409083646\,T^{-3}$
Y_2O_3 (S2)	-1913286	82.75	131.796

Table A-II – Thermodynamic properties of the stoichiometric compounds

Compound	ΔH°_{298} (J)	S°298 (J/K)	Cp (J/K)
YAG	-14711422.0	366.34	$1170.478 - 19306815T^{-2} - 4141.93T^{-1/2} + 2045418230\ T^{-3}$
YAP	-3741715.6	99.56	$286.814 - 3861363T^{-2} - 828.3869T^{-1/2} + 409083646\ T^{-3}$
YAM	-5745748.1	156.31	$418.61 - 3861363T^{-2} - 828.3869T^{-1/2} + 409083646\ T^{-3}$
Y_2O_3 (S1)	-1982194.0	57.40	131.796
27R	-3681248.4	307.702	$507.93 - 15519838.24T^{-2} - 55027\ T^{-1} + 797.468\ T^{-1/2} + 2513618218\ T^{-3}$
21R	-3052096.02	238.446	$407.101 - 4694110.32T^{-2} - 39309.78\ T^{-1} + 332.938\ T^{-1/2} + 1912322626\ T^{-3}$
12H	-2749469.8	232.778	$356.685 - 10523348.85T^{-2} - 31447.82T^{-1} + 100.673\ T^{-1/2} + 1611674830\ T^{-3}$

Table A-III – Thermodynamic data for liquid AlN-Al_2O_3-Y_2O_3 system

Component	Component No.	G°
AlN	1	G° of AlN (S1) *from* [30] + $\Delta G^{\circ}_{fusion}$ where $\Delta G^{\circ}_{fusion}$= 70557.8 – 23.0055 T
Al_2O_3	2	G° of Al_2O_3 (S4) *from* [30] + $\Delta G^{\circ}_{fusion}$ where $\Delta G^{\circ}_{fusion}$= 87918.58 – 37.847 T
Y_2O_3	3	G° of Y_2O_3 (S2) *from* [30] + $\Delta G^{\circ}_{fusion}$ where $\Delta G^{\circ}_{fusion}$= 68908.00 – 25.340 T

Table A-IV – Binary excess mixing terms

Parameter	M	N	I	J	A	B	C
1	1	2	1	1	-40061.00	0.0	0.0
2	1	2	2	1	29119.00	0.0	0.0
3	1	3	1	1	-57164.00	0.0	0.0
4	1	3	2	1	36945.00	0.0	0.0
5	2	3	1	1	-167230.00	0.0	0.0
6	2	3	1	2	-39366.00	0.0	0.0

Table A-V – Thermodynamic data for γ-spinel phase

Component	Component No.	G°
AlN	1	G° of AlN (S1) *from* [30] + $\Delta G^{\circ}_{fusion}$ where $\Delta G^{\circ}_{fusion}$ = 52500.15 – 13.355 T
Al_2O_3	2	G° of Al_2O_3 (S4) *from* [30] + $\Delta G^{\circ}_{fusion}$ where $\Delta G^{\circ}_{fusion}$ = 64500.48 – 25.847 T

Table A-VI – Binary excess mixing terms for γ-spinel solution

Parameter	M	N	I	J	A	B	C
1	1	2	1	1	-171499.0	38.00	0.0
2	1	2	2	1	438695.1	-151.17	0.0